AJNR

Integral and shell-MIP display algorithms in MR and CT three-dimensional models of the brain surface.

S O Casey, D Rubinstein, K O Lillehei, R A Alberico, R R Ozsvath, A G Cajade-Law, B E Weprin, E Michel and C L Truwit

AJNR Am J Neuroradiol 1998, 19 (8) 1513-1521
http://www.ajnr.org/content/19/8/1513

AJNR Am J Neuroradiol 19:1513–1521, September 1998

Integral and Shell-MIP Display Algorithms in MR and CT Three-dimensional Models of the Brain Surface

Sean O. Casey, David Rubinstein, Kevin O. Lillehei, Ronald A. Alberico, Robert R. Ozsvath, Ana G. Cajade-Law, Bradley E. Weprin, Eduard Michel, and Charles L. Truwit

BACKGROUND AND PURPOSE: **Our purpose was to demonstrate the use of integral and shell maximum intensity projection (shell-MIP) display algorithms in the 3-D CT and MR depiction of cerebral gyral and surface venous anatomy and disorders. These new algorithms are compared against MIP and shaded-surface-display (SSD) algorithms.**

METHODS: **Integral and shell-MIP displays were generated from a specified number of proximal surface voxel layers in a 3-D model. Algorithmic models were compared on nine contrast-enhanced spoiled gradient-recalled acquisition in a steady state (SPGR) MR venograms for brain surface anatomic identification and detail. Seven CT venograms were compared for conspicuity of filling defects. Twelve contrast-enhanced preoperative planning 3-D MR models were rated for neurosurgical utility.**

RESULTS: **A shell-MIP score of 7.00 and an integral score of 6.78 represented the highest mean subjective MR gyral quality (1–10 scale) followed by an SSD score of 3.89 and an MIP score of 1.06. Mean confidence scores for MR central sulcus identification (1–10 scale) were shell-MIP, 7.67; integral, 7.00; SSD, 3.22; and MIP, 1.00. Mean superficial venous quality MR ratings (1–10 scale) were shell-MIP, 8.22; MIP, 7.39; integral, 7.00; and SSD, 3.72. The mean number of cortical veins draining into each side of the superior sagittal sinus on MR was as follows: MIP, 6.19; integral, 6.06; shell-MIP, 5.94; and SSD, 3.81. Mean confidence scores for filling defect identification on CT venograms (1–5 scale) revealed a shell-MIP score of 4.36 and an integral score of 4.29 to be superior to a MIP score of 3.00. In selected cases, 3-D presurgical planning, prior to tumor resection, was clinically useful.**

CONCLUSION: **Integral and shell-MIP are useful 3-D display algorithms for simultaneous display of superficial cerebral veins and gyri on MR images and of thrombosis on CT venograms.**

To date, three-dimensional (3-D) models of the brain surface have been used in selected cases for evaluating the cerebral venous system and for displaying gyri and sulci, especially in preoperative planning (1–7). Noninvasive display of the superficial dural sinuses and cortical veins is typically rendered with a maximum intensity projection (MIP) algorithm to create MR (8) or CT (9) venograms. On the other hand, most of the efforts to display 3-D images of the brain surface gyri and sulci have used MR data sets displayed with the shaded-surface-display (SSD) algorithm (1–4) or with volume-rendering algorithms (5–7) using a reflected artificial light source. We present two display algorithms, integral and shell-MIP, that are each well suited for the simultaneous display of superficial cerebral veins and gyri.

Received April 22, 1997; accepted after revision April 1, 1998.

From the Departments of Radiology (S.O.C., E.M., C.L.T.) and Neurosurgery (B.E.W.), University of Minnesota Medical School, Minneapolis; the Departments of Radiology (D.R., A.G.C.) and Neurosurgery (K.O.L.), University of Colorado Health Sciences Center, Denver; the Department of Radiology, Brigham and Women's Medical Center, Boston, MA (R.A.A); and the Department of Radiology, Long Island Jewish Medical Center, New Hyde Park, NY (R.R.O.).

Address reprint requests to Sean O. Casey, MD, Department of Radiology, University of Minnesota Medical School, Box 292, 420 Delaware St SE, Minneapolis, MN 55455.

Methods

Acquisition

MR and CT volumetric studies were performed typically for the evaluation of dural sinuses or for preoperative planning.

MR data sets were acquired with a 1.5-T MR imager in 17 subjects. A T1-weighted 3-D spoiled gradient-recalled acquisition in a steady state (SPGR) volume was acquired in the axial plane with the following parameters: 32/13/1 (TR/TE/excita-

tions), 35° flip angle, 256 × 192 matrix, 22 × 16.5-cm field of view, and first-order gradient moment nulling. Imaging was performed immediately after IV injection of gadopentetate dimeglumine (0.1 mmol/kg) in 24 patients. Acquisition time for a 60-section slab of supratentorial brain with 0.8- to 1.3-mm-thick partitions was 4:58 minutes. Whole-brain coverage was obtained using the same parameters, except for 0.75 excitations and 124 partitions, for an acquisition time of 7 minutes. At the request of the operating neurosurgeon, a subset of 12 patients were imaged for preoperative planning on the morning of surgery with at least four MR fiducial markers stuck to the scalp. Data were transferred to an operating room workstation for the purpose of intraoperative frameless stereotactic localization with a robotic microscope (MKM System, Carl Zeiss, Inc, Thornwood, NY) in eight of the 12 patients. Supplementary integral and shell-MIP models were provided for brain surface mapping, and intraoperative correlation was obtained in all 12 cases. Five other MR data sets were used for algorithmic comparisons, including studies from one volunteer who did not receive contrast material, three patients who were being examined for elevated CSF pressure (and suspected cerebral venous hypertension), and one patient being examined for chronic dural sinus thrombosis.

CT data sets consisted of 17 cerebral CT venograms obtained for suspected dural sinus thrombosis. Findings on four CT venograms were diagnosed as dural sinus thrombosis. Ninety milliliters of nonionic contrast material (300 mg I/mL) was infused intravenously at a rate of 2.8 mL/s for the first 60 mL followed by a rate of 1.0 mL/s for the final 30 mL. One-millimeter collimated helical scans with a 2:1 pitch (2.0 mm/s table speed) were obtained 30 seconds after the start of infusion of contrast material by scanning from the skull vertex to the base. Total coverage was 118 mm for a single helical acquisition of 60-seconds duration. Scanning parameters included 120 kVp, 220 mA, and a 22-cm display field of view. The raw data were reconstructed to 148 overlapping images at 0.8-mm intervals before their use in 3-D reformations.

Model Preparation

Three-dimensional models for both CT and MR studies were generated on an Advantage Windows 3-D workstation (General Electric Medical Systems, Milwaukee, WI). Prior to the application of integral or shell-MIP algorithms, each 3-D model was manually segmented on the workstation to isolate the brain, with its associated veins and sulcal CSF, from overlying tissues. First, a primary 3-D model was created, consisting of all voxels from the source images. Next, a bone mask was created by thresholding and was then subtracted from the primary model. For CT, this subtraction mask was a high-density bone model. For MR imaging, this subtraction mask consisted of a low-intensity bone model that also included air and some CSF. The bone mask was then dilated in thickness by single-voxel-layer increments and sequentially subtracted from the primary model until the scalp and residual calvaria were no longer in contact with the brain and could be discarded. The isolated brain model, along with surface veins and CSF, was then displayed with the integral algorithm. For MR imaging, further processing was performed to improve sulcal and venous detail. A "close-gaps" function returns inadvertently subtracted sulcal CSF to the model. A duplicate brain model was then created and dilated by approximately four voxel layers. This was thresholded to select for high-intensity vascular voxels that were then added back to the primary brain model, thus eliminating any accidental superficial venous deletions.

Three-dimensional Surface Algorithms

The GE workstation allows quick switching within seconds between its integral, MIP, and SSD algorithms. The integral display algorithm depicts the average intensity value of the first five voxels deep to the model surface that is nearest to the viewer in any chosen projection (10). Presently, the integral algorithm is available commercially on the GE Advantage Windows 3-D workstation. MIP projects intensity onto the screen that is the highest in the 3-D model volume along each ray perpendicular to the viewing screen (11). Shell-MIP, on the other hand, applies this same MIP algorithm to a user-specified number of outer voxel layers extracted from the model surface. Unlike in conventional MIP models, high-intensity voxels deep within the shell-MIP model are discarded and not displayed. The shell-MIP algorithm is not proprietary on the GE workstation but is created by the "extract surface" function of the workstation, which allows the user to select an optimal number of voxel layers (usually three to five) in a surface shell extracted from the model. Unlike with the proprietary integral algorithm, cutaway views are needed with the shell-MIP algorithm to temporarily remove the far sides of the models and thus to prevent overlapping surfaces. This semiautomated application of the shell-MIP algorithm to a segmented model can be performed in less than 1 minute. The entire CT/MR postprocessing—including 3-D model generation, segmentation, and algorithm application—typically requires 10 minutes and is presently specific to the GE Advantage Windows 3-D workstation. Transfer of data to the workstation in addition to the filming of multiple projections and cine loops requires additional time. Complex preoperative planning of cases involving tumors deep to the surface required some additional segmentation. Scalp fiducial markers could also be superimposed on the brain model to assist in craniotomy site planning. These two additional segmentations could raise total postprocessing time to 15 to 30 minutes.

Evaluation

Three-dimensional brain models of a subset of nine contrast-enhanced MR data sets were independently compared in integral, shell-MIP, standard MIP, and SSD algorithms by two neuroradiologists blinded to the intent of the study and unfamiliar with the new surface algorithms. Studies that showed disease significantly distorting or involving the brain surface were excluded from the MR comparison, as was the single noncontrast MR study. The qualifying studies were ranked as to the quality of superficial venous and gyral depiction on a scale of 1 to 10 (with 10 representing the highest quality). Additionally, the level of confidence in the identification of the central sulcus on each side was recorded on a scale of 1 to 10 (with 10 designating the greatest confidence). The number of superficial cortical veins draining from each cerebral hemisphere into the superior sagittal sinus was also recorded. Three-dimensional models of a subset of seven CT venograms with known dural sinus or cortical venous filling defects (four cases with thrombus and three with large arachnoid granulations) were compared in integral, shell-MIP, and standard MIP display algorithms. These were ranked for the conspicuity of the defects on a scale of 1 to 5 (with 5 denoting the greatest conspicuity). One case of acute thrombosis in which source data were no longer available and two additional follow-up studies of chronic thrombosis in the same patient were excluded. Statistical significance between the different algorithms was determined as a P value of .05 by means of the paired, two-tailed Student's t-test.

To gauge the subjective utility of the 12 3-D models for preoperative planning in neoplasm resection, a questionnaire was completed by a single neurosurgeon who was provided with the case information and images. The surgeon was asked to rank the utility of the cortical venous map, the gyral map, and the combined venous and gyral map. The surgeon also ranked the utility of the model in planning craniotomy site and size, as well as localizing the tumor (utility for planning the surgical approach). These subjective utilities were ranked on a scale of 1 to 5 (with 5 representing very useful, 3 denoting somewhat helpful, and 1 signifying not useful). For nine cases, 3-D models were only supplementary to frameless or frame-based stereo-

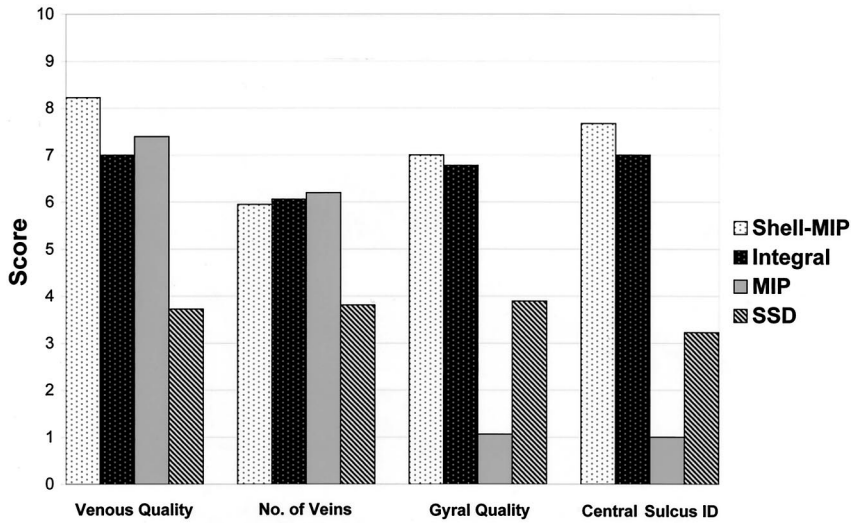

FIG 1. Nine contrast-enhanced SPGR 3-D MR models with normal brain surfaces were compared in four different display algorithms. Tested qualities included overall superficial venous and gyral qualities as well as confidence in the ability to identify the central sulcus. The mean scores were charted on a 1–10 scale (with 10 representing the greatest quality or confidence). The number of cortical veins directly draining into the superior sagittal sinus on each separate side was also counted. Shell-MIP and integral algorithms excelled in all four features.

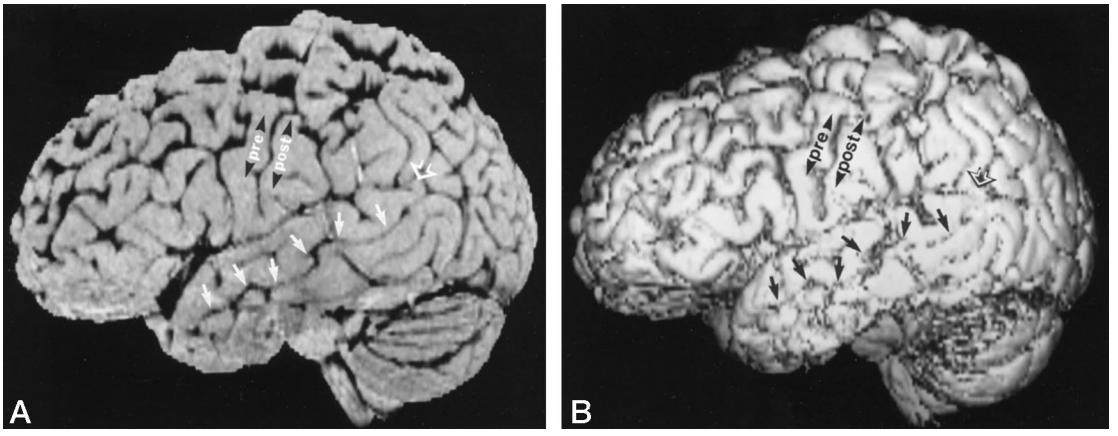

FIG 2. 3-D models generated from an unenhanced T1-weighted SPGR MR image in a healthy 25-year-old woman. Dural sinuses and cortical veins have been mostly removed by workstation editing.

A, Integral display from left lateral viewpoint. Note the sylvian fissure, the superior temporal sulcus (*solid arrows*), the angular gyrus (*open arrow*), the precentral gyrus (pre), and the postcentral gyrus (post).

B, SSD from left lateral viewpoint. Gyral patterns are less well appreciated on the SSD model, especially in the temporal and occipital lobes and the cerebellum.

tactic guidance. This was taken into account in the rating of the utilities of these models. For these nine cases, additional rankings were made under an assumption that 3-D models and conventional MR images were the only form of guidance at the time of surgery; that is, it was assumed that frameless stereotactic equipment or intraoperative interventional MR imaging was not available.

Results

The integral and shell-MIP models displayed relative voxel intensity differences between veins, gyri, and sulci while providing sufficient 3-D cues.

Gyral Display

Subjectively, shell-MIP and integral display algorithms had the highest mean gyral quality rankings at 7.00 and 6.78, respectively. This difference between shell-MIP and integral was not significant ($P = .58$), although the difference between integral and SSD at 3.89 was significant ($P < .01$). As expected, standard MIP had the lowest mean gyral quality ranking at 1.06 (Fig 1). While sulcal detail was often similar among integral, shell-MIP, and SSD algorithms for displaying the frontal and parietal lobes viewed from above, integral and shell-MIP displays were subjectively superior to SSD for depicting the smaller sulci on the surface of the temporal and occipital lobes (Fig 2). Identification of the central sulcus was easier with shell-MIP (7.67) and integral (7.00) models than with SSD (3.22) or standard MIP (1.00) models. The difference between the shell-MIP and integral models was significant ($P = .02$), and both these algorithms provided significantly greater confidence in central sulcus identification than did the SSD model.

Venous Display

With contrast-enhanced MR imaging, dural sinus and cortical venous detail with shell-MIP and integral models was excellent, with mean quality scores of 8.22 and 7.00, respectively (Fig 3). Subjectively, shell-MIP

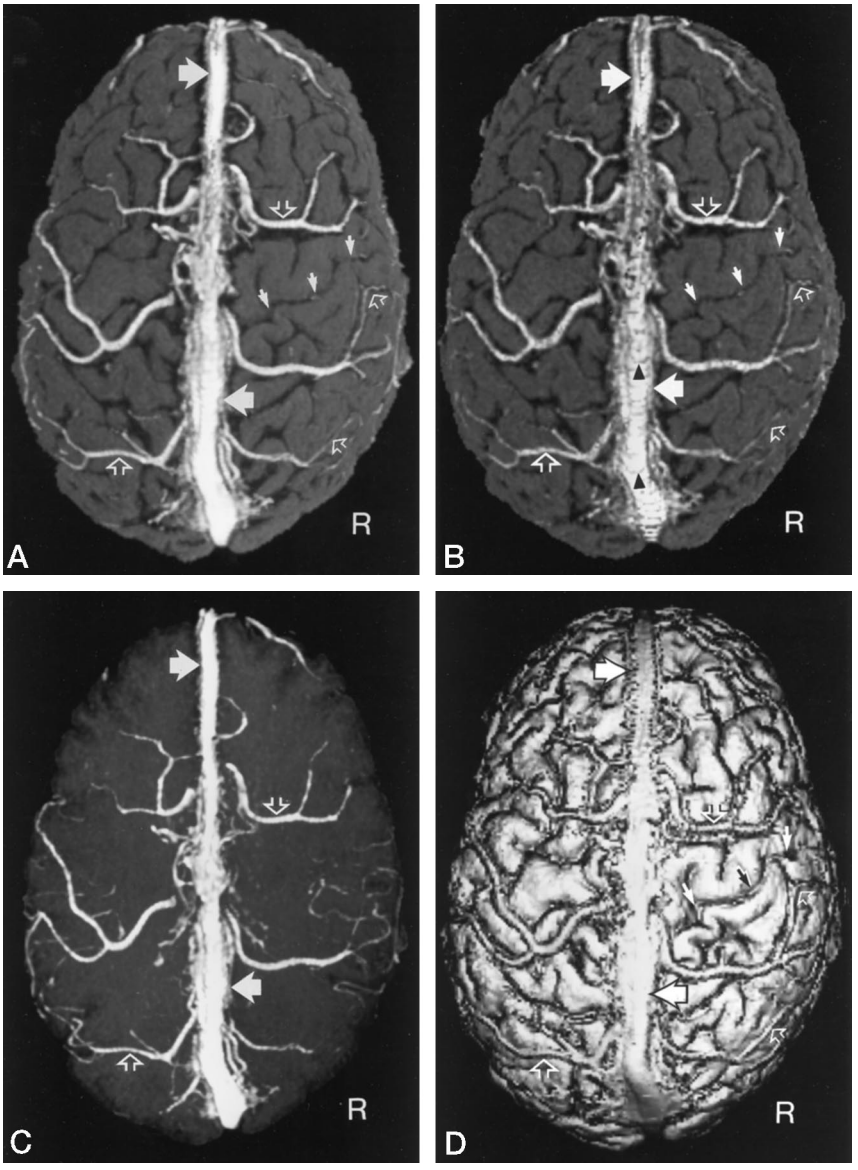

FIG 3. Different 25-year-old woman with normal brain surface. These axial 3-D images, reconstructed from a contrast-enhanced SPGR MR image, are viewed as if looking down at the vertex of the patient's head. Since integral and shell-MIP displays are surface views, the left and right sides of the models appear reversed relative to the accepted radiologic convention for 2-D cross-sectional images. This orientation is advantageous in preoperative planning, since it corresponds to the surgical viewpoint.

A, Shell-MIP display shows that the superior sagittal sinus (*large solid arrows*) and cortical veins (*large open arrows*) are bright relative to the brain surface. Some small cortical veins (*small open arrows*) are seen better on shell-MIP and integral displays than on the conventional MIP display. Note the right central sulcus (*small solid arrows*). The left central sulcus is partly obscured by an overlying cortical vein. R = right.

B, Integral display provides similar gyral detail but venous display is somewhat coarse and reveals more section edge artifact (stair-stepping) (*black arrowheads*).

C, Conventional MIP display, with the inferior of the model cut away, provides good venous detail but is lacking in 3-D effect and gyral display. R = right.

D, With SSD, the cortical and venous detail is present but more laborious to discern than on integral and shell-MIP displays.

was preferred slightly over integral by both readers in four of nine cases, owing to the smooth venous detail. This difference in mean subjective venous quality was significant ($P < .01$). Full-volume standard MIP received a mean quality score of 7.39 for superficial cerebral venous display. Shell-MIP was significantly superior to standard MIP ($P = .02$) but there was no statistically significant difference in venous quality between standard MIP and integral models ($P = .39$). Standard MIP models were limited by overlapping vascular structures and noise within the interior of the model that tended to decrease small-vessel detail as compared with shell-MIP models. Despite generally good venous detail, SSD models had the lowest mean venous display quality, with a score of 3.72. SSD models appeared limited by having too many structures with similar gray scale values, making it more laborious to distinguish veins from sulci. The mean number of cortical veins draining into each separate side of the superior sagittal sinus for each of the display algorithms was counted as follows: MIP, 6.19; integral, 6.06; shell-MIP, 5.94; and SSD, 3.81. The difference between MIP, integral, and shell-MIP in the number of superficial cortical veins seen was not significant ($P = .22$).

Detection and delineation of intraluminal venous filling defects on CT venograms was best with the integral and shell-MIP displays (Fig 4). In the five CT venograms with dural sinus thrombosis, shell-MIP and integral provided a clearer depiction of the margins of intraluminal thrombus than did MIP, with respective mean filling defect conspicuity ratings of 4.36, 4.29, and 3.00 (Fig 5). While the difference between shell-MIP and integral was not significant ($P = .336$), both algorithms were significantly superior to standard MIP for the identification and delineation of filling defects ($P < .01$). In two patients with superior sagittal sinus thrombosis, extension of the thrombus into cortical veins was directly depicted on integral and shell-MIP models as relatively lower-density venous segments in comparison with higher-density normal venous segments. These cortical vein

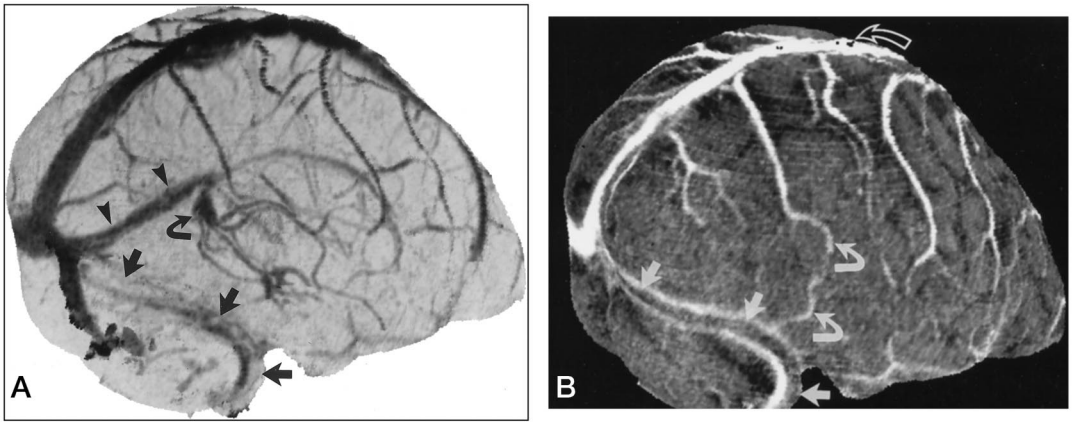

FIG 4. Helical CT venogram in a 74-year-old woman with suspected dural sinus thrombosis on MR images obtained 10 days earlier.
A, MIP model from right posterior oblique view reveals decreased density in the right transverse and sigmoid sinuses (*straight arrows*). The straight sinus (*arrowheads*) and vein of Galen (*curved arrow*) are seen within the interior of the model. A = anterior.
B, Integral model from same view shows filling defect from thrombus in right transverse and sigmoid sinuses (*straight arrows*). The deep cerebral venous system in the interior of the model is not displayed by integral algorithm. Several right-sided cortical veins are seen better on the integral model as compared with MIP (*solid curved arrows*). Note the small areas of signal void (*open curved arrow*) in the superior sagittal sinus near the brain vertex. This is a typical location for these artifacts, which are probably related to aliasing. A = anterior.

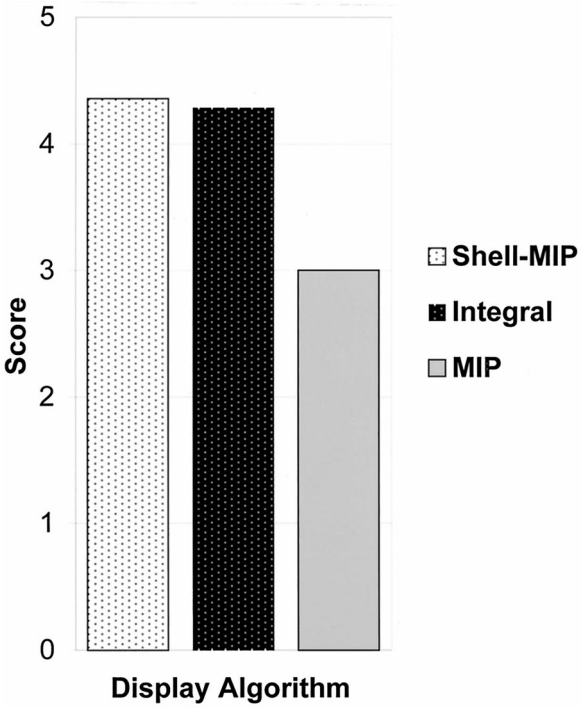

FIG 5. Comparison of differing display algorithms for seven 3-D CT venograms with known filling defects due to thrombi or large arachnoid granulations. The mean scores for the two observers are charted on a 1–5 scale (with 5 representing the greatest filling defect conspicuity).

thrombi had not been appreciated prospectively on source images and were virtually undetectable even in retrospect on the 3-D standard MIP models other than for the indirect finding of nonvisualization of the involved veins. Another patient with thrombosis of the right transverse and sigmoid sinuses had extension of thrombus into the right vein of Labbé, which was directly visualized on the integral and shell-MIP displays as a filling defect. Intrasinus septa of the superior sagittal sinus in two patients, as well as arachnoid granulations in two other patients, were also best seen on 3-D CT venographic models using the integral and shell-MIP display algorithms.

Preoperative Planning and Intraoperative Correlation

Integral and shell-MIP display of the contrast-enhanced SPGR MR studies and CT venograms also proved useful to varying degrees for preoperative planning in 12 selected patients prior to resection of brain neoplasm (Table). Both integral and shell-MIP algorithms proved to be adequate for combined venous and gyral mapping in a single display. The mapping was most frequently requested for tumors requiring an interhemispheric approach or for those near the sensorimotor cortex or in proximity to the superior sagittal sinus (or major cortical veins). It was confirmed intraoperatively that virtually all cortical veins down to 1 mm in width were depicted on the integral and shell-MIP models. Cortical venous mapping eliminated the need for preoperative catheter digital subtraction angiography in two patients and was considered helpful to a degree in all our cases. Easy identification of the central sulcus on the gyral maps was helpful to our neurosurgeons in several cases. In one patient, the location of the precentral and postcentral gyri on the integral and shell-MIP models was confirmed as the location of the motor and sensory cortices by intraoperative electrostimulation (Fig 6). Superficial tumors, with at least some contrast enhancement within five voxels of the brain surface, could be visualized on the 3-D integral and shell-MIP images on eight MR images and two CT studies. In these cases, the relationship of tumor to veins (on MR or CT studies) and gyri (on MR studies) was well depicted. To visualize deep tumors, it was necessary to perform segmentation and superimposition of tumor models on the integral and shell-MIP images. With SSD models, both superficial and

Preoperative surgical planning using 3-D SPGR MR models with shell-MIP and integral algorithms

Patient	Tumor	Location	Guidance	Subjective Surgical Utility (1–5 scale, 1 = not useful, 5 = very useful)				
				Venous Map	Cortical Map	Craniotomy Site/Size	Tumor Localization	Overall
1	Recurrent hemangiopericytoma	Invading middle ⅓ of SSS, Midline frontoparietal (SMC)	Images alone	5*	5	3	3	4
2	Small meningioma	Right parietal, adjacent to SSS	Frameless	5 (5)	2 (5)	1 (4)	2 (3)	3 (4)
3	Anaplastic oligodendroglioma	Left frontoparietal (SMC)	Frameless	5 (5)	2 (5)	1 (4)	2 (4)	3 (4)
4	Large meningioma	Pineal cistern, surrounded by ICVs and BVRs, IHF approach	Frameless	5 (5)	2 (2)	1 (1)	2 (2)	2 (3)
5	Large solitary colon carcinoma metastasis	Medial left posterior frontal/cingulate, IHF approach	Images alone	5	5	4	5	5
6	Large high-grade astrocytoma	Left parietal	Frameless	3 (3)	2 (4)	1 (4)	2 (4)	2 (4)
7	Giant meningioma	Invading middle ⅓ of SSS, bilateral frontoparietal (SMC) encasing multiple cortical veins	Images alone	4*	5	1	1	4
8	Solitary adenocarcinoma metastasis	Right medial superior frontal	Frameless	5 (5)	3 (3)	1 (4)	1 (4)	2 (4)
9	Meningioma	Right posterior frontal (MC)	Frameless	5 (5)	4 (5)	1 (4)	1 (3)	3 (4)
10	Large oligodendroglioma	Right medial frontoparietal (SMC)	Frameless	5 (5)	4 (5)	1 (4)	2 (4)	3 (4)
11	Solitary lung carcinoma	Left medial frontal	Frameless	5 (5)	2 (2)	1 (4)	1 (4)	3 (4)
12	Astrocytoma	Right posterior frontal (MC)	Frame biopsy	5 (5)	3 (5)	1 (4)	1 (4)	3 (4)

Note.—For cases in which frameless (or frame-based) stereotaxy was used, the first utility ratings assume the actual case conditions. These are followed by additional values within parentheses. These second utility rankings assume that 3-D models and conventional MR images were the only form of guidance at the time of surgery; ie, it was assumed that frameless stereotactic equipment or intraoperative interventional MR imaging was not available. SSS indicates superior sagittal sinus; SMC, presumed sensorimotor cortex; ICVs, internal cerebral veins; BVRs, basal veins of Rosenthal; IHF, interhemispheric fissure approach; MC, presumed motor cortex. Frameless indicates MKM frameless stereotaxic system.

* Without venous maps, conventional digital subtraction angiograms would have been obtained for venous evaluation.

deep tumors were not directly visible and required segmentation with superimposition of tumor models on the original model for tumor visualization in all cases. While even deeper contrast-enhancing tumors can be seen on conventional MIP displays, the relation of surface sulci, such as the central sulcus, to these lesions cannot be appreciated.

In selected cases, 3-D models of the scalp with fiducial markers were superimposed on the integral and shell-MIP brain models to assist in craniotomy planning. The utility of the 3-D models for craniotomy site and size, as well as for tumor localization, tended to be reduced by the simultaneous use of stereotactic guidance techniques. Integral and shell-MIP were also able to reveal compression of sulci from edema surrounding some of the tumors. In our experience, large amounts of edema surrounding neoplasm were found to focally limit the quality of the MR gyral and venous maps with all the tested display algorithms.

Discussion

The integral algorithm displays the average intensity of a five-voxel-deep layer along the proximal surface, thus essentially providing the viewer with a five-voxel-thick curved reformation over a predetermined 3-D surface. The integral image could also be considered to represent a nonplanar section five voxels thick, in our case, contoured to the brain surface. Shell-MIP is an ordinary MIP algorithm, only it is targeted to a small volume of interest limited to a specified number of voxels along a model surface. The essential difference between the two algorithms is that, while the integral algorithm displays intensity data contributed from every voxel less than or equal to five deep from the surface, the shell-MIP algorithm uses only intensity data from the single most intense of these superficial voxels. The visible result is that the shell-MIP image provides the best visualization of such high-intensity structures as blood vessels, even if small and faintly visible on the source images. The integral image often appears to have slightly more noise but is at least theoretically better able to simultaneously display low-intensity surface features, such as sulci. Shell-MIP models, unlike integral models, presently require manual extraction of a surface shell and cut-plane view to avoid simultaneous application of the MIP algorithm to both the proximal and far sides of the brain shell. Future improvements in software should easily automate these processes and, as with the integral algorithm, avoid the need to discard the nondisplayed interior data of the model.

To date, the main uses of 3-D surface display of the brain gyri and sulci include preoperative planning (3, 4, 6, 12, 13) (often in conjunction with functional MR

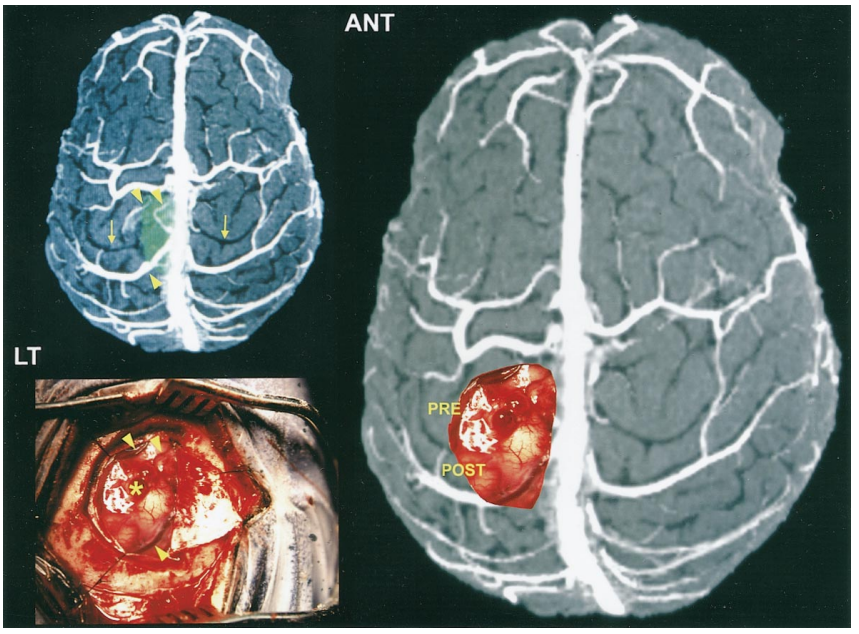

FIG 6. 30-year-old man examined 1.5 hours before surgery for left posterior frontoparietal lobe anaplastic oligodendroglioma.

Top left. Axial 3-D shell-MIP image, reconstructed from a contrast-enhanced SPGR MR image, emulates the intraoperative viewpoint and displays the superior sagittal sinus and cortical veins as bright relative to brain surface. The tumor below the surface has been separately segmented and colored green. Note the central sulci (*yellow arrows*) and several small cortical veins (*yellow arrowheads*) overlying the tumor. Even with segmentation of the tumor, this model was generated in under 15 minutes postprocessing time while the patient was en route to the operating room.

Bottom left. Intraoperative photo just after the dura was peeled away. The 3-D shell-MIP model corresponds well with the small cortical veins (*yellow arrowheads*) overlying the tumor. A previous biopsy site is visible (*yellow asterisk*).

Right. Surgical field superimposed on 3-D shell-MIP model for correlative purposes. Intraoperative electrostimulation confirmed the predicted location of the precentral (PRE) and postcentral (POST) gyri on the 3-D MR model with the true motor and sensory cortices. LT = left, ANT = anterior.

or magnetic source imaging) and display of gyral anomalies (14, 15). The most commonly used technique for brain surface display is workstation generation of 3-D models from thin-section 3-D gradient-echo MR studies, which are typically displayed with the SSD algorithm.

Integral and shell-MIP algorithms offer improvements over previously reported methods for depiction of the brain surface in selected cases. Preparation of SSD models requires direct delineation of the brain-CSF interface by time-consuming manual or automatic editing methods in order to isolate the brain from the overlying CSF. Volume-rendered models, as reported to date, have used similar editing methods. After surface selection, often by thresholding, the SSD algorithm discards original voxel intensity data and depicts only surface contours. SSD MR models yield acceptable gyral detail in older patients with large sulci, but are sometimes limited for gyral display in younger patients. Integral and shell-MIP, on the other hand, can provide improved gyral display in patients with small sulci, because the low-intensity CSF in the sulci yields sharp contrast relative to adjacent high-intensity gyri. Preparation of integral and shell-MIP models only requires determination of the surrounding bony calvaria and can be completed in less than 10 minutes. This editing only indirectly approximates the brain surface, and thus any CSF in proximity to the brain surface remains within these integral and shell-MIP models. Like integral and shell-MIP, some newer volume-rendering algorithms can provide relative surface voxel intensities in their 3-D displays. It is likely that the advantages of integral and shell-MIP algorithms will also apply to these volume-rendering algorithms, provided they are customized to confine their display to just a few layers of surface voxels and that sulcal CSF is left in place during postprocessing. Depiction of gyri on the undersurface of the brain along the skull base, however, remains limited on all tested algorithms, owing to bony irregularity, which causes difficulty in obtaining an accurate representation of the brain–skull base interface during model segmentation.

Integral and shell-MIP models offer improved visualization of the superficial cerebral venous system. To date, display of surface venous anatomy has been performed by using the venous phase of digital subtraction angiography, MR venography with MIP display (8), or CT venography with MIP display (9). Although the venous display can be adequate with these techniques, digital subtraction angiography is invasive and all these methods have limited 3-D effect and no gyral anatomic information. SSD models provide limited venous conspicuity, since without manual segmentation and coloration of the superficial cerebral veins they cannot display the relatively higher intensities of the contrast- or flow-enhanced veins. Shell-MIP models were judged superior to conventional MIP for superficial venous display in this study, most likely because this new algorithm eliminates competition from noise in the model interior and avoids overlap from deeper vascular structures. Use of integral and shell-MIP algorithms has changed our sequence requirements for MR venography. Unlike standard time-of-flight (TOF) MR venography displayed with MIP, contrast-enhanced MR venography displayed with integral or shell-MIP algorithms eliminates the need for saturation bands and allows more freedom in the choice of acquisition plane. The axial plane was preferred, since this applied the greatest in-plane resolution to the middle third of the superior sagittal sinus and to the most important of the cortical veins, which could be efficiently imaged in a supraventricular 3-D SPGR slab. Furthermore, for pre-

operative planning, the superior viewpoint of the brain vertex also best emulated the typical surgical approach and most neoplasms could be included in the imaging volume. Unlike in TOF MR venography, inferior saturation bands (to prevent arterial TOF effects) are unnecessary, since integral and shell-MIP models already select for just the veins on the model surface.

Preoperative planning studies were typically requested by our neurosurgeons for selected complex cases in which lesions were located in proximity to the sensorimotor cortex or adjacent to the superior sagittal sinus. While the commonly performed 2-D TOF MR venography provides reasonable venous detail, typical acquisition sequences are tailored for MIP display with saturation of signal from stationary brain parenchyma. Two-dimensional TOF sequences alone do not provide adequate parenchymal evaluation and thus preoperative planning studies in patients with neoplasm usually require an additional T1-weighted sequence following intravenous administration of contrast material to visualize enhancing brain lesions. Our contrast-enhanced SPGR MR studies with integral or shell-MIP display were useful for preoperative planning, since they can be used as the only required sequence for both venous and parenchymal depiction and provide clinically useful T1-weighting on the source images and reformations. Integral and shell-MIP displays have a further advantage over SSD as preoperative planning surface algorithms in that they can directly show superficial contrast-enhancing lesions. SSD algorithms, on the other hand, can only depict the distortion or flattening of sulci of the brain surface from a superficial lesion; they cannot directly illustrate the contrast enhancement of the lesion. It is hoped that the preoperative display of the variable cortical venous anatomy will decrease the risk of venous infarction. Furthermore, if intraoperative brain shifting causes frameless stereotactic equipment to become inadequate, correlation of the brain surface with the venous and gyral maps may be useful for surgical guidance.

The present use of MIP in MR and CT venography to depict intraluminal abnormalities in cerebral venous thrombosis is less than ideal. MIP selects the most intense voxel within a vessel while sacrificing lesser-intensity voxels within the same vessel or other vessels. Thus, intraluminal thrombus may be obscured or underestimated in size if surrounded by flowing blood on MR images (11, 16) or by denser contrast-enhanced blood on CT scans. This occurs to a far lesser degree with integral display, since it is an average of voxels, with lower-intensity voxels also contributing to the final display. In our study, the shell-MIP and integral algorithms provided the best 3-D CT venographic demonstration of filling defects in superficial dural sinuses. Shell-MIP performed better than was theoretically expected, most likely because dural sinus thrombi are typically in contact with a substantial portion of the vessel wall and usually are not predominantly free-floating.

The display of cortical venous thrombosis in three cases in our series of CT venograms showing dural sinus thrombosis suggests that integral display may allow detection of the uncommon but presumably underdiagnosed condition of isolated cortical vein thrombosis, for which there is presently no ideal noninvasive test (17). Our results suggest that CT venography with integral display can depict at least some cases of cortical venous thrombosis by directly visualizing discrete lower-density venous segments or filling defects adjacent to normally enhancing venous segments. Further study will be needed to determine the sensitivity and specificity of the integral algorithm in the CT venographic diagnosis of cortical vein thrombosis.

Two potential artifacts have been observed with our methods that are not inherent to the integral or shell-MIP algorithms themselves but are related to model segmentation. Signal voids, not present in the original data set, can appear, especially if the close-gaps function of the workstation is applied excessively (Fig 4B). These typically occur near the vertex in the midline over high-intensity structures, such as the superior sagittal sinus, and are easily differentiated from disease by their total absence of signal. This artifact is probably related to aliasing and may be workstation-specific. The second type of postprocessing artifact originates from difficulties in subtracting high-density bone from high-density veins on CT venograms and can result in small cortical venous deletions regardless of the display algorithm.

Conclusion

Application of the integral and shell-MIP algorithms is presently limited to selected cases. At our institutions, we use these algorithms for the display of CT venograms obtained in cases of suspected cerebral venous thrombosis and in certain MR or CT preoperative planning studies, predominantly for venous mapping prior to tumor resection.

Acknowledgments

We thank the technologists in the MRI and CT units at the University of Colorado Health Sciences Center for scanning patients and Glenn Kindt for coordinating the intraoperative photographic correlation in some of the patients.

References

1. Cline HE, Dumoulin CL, Hart HR Jr, Lorensen WE, Ludke S. **3D reconstruction of the brain from magnetic resonance images using a connectivity algorithm.** *Magn Reson Imaging* 1987;5:345–352
2. Cline HE, Lorenson WE, Kikinis R, Jolesz F. **Three-dimensional segmentation of MR images of the head using probability and connectivity.** *J Comput Assist Tomogr* 1990;14:1037–1045
3. Jack CR Jr, Marsh WR, Hirschorn KA, et al. **EEG scalp electrode projection onto three-dimensional surface rendered images of the brain.** *Radiology* 1990;176:413–418
4. Kikinis R, Langham Gleason P, et al. **Computer-assisted interactive three-dimensional planning for neurosurgical procedures.** *Neurosurgery* 1996;38:640–649
5. Levin DN, Hu X, Tan KK, Galhotra S. **Surface of the brain: three-dimensional MR images created with volume rendering.** *Radiology* 1989;171:277–280
6. Hu X, Tan KK, Levin DN, et al. **Three-dimensional magnetic**

resonance images of the brain: application to neurosurgical planning. *J Neurosurg* 1990;72:433–440
7. Kesava P, Baker E, Mehta M, Turski P. **Staging of arteriovenous malformations using three-dimensional time-of-flight MR angiography and volume-rendered displays of surface anatomy.** *AJR Am J Roentgenol* 1996;167:605–609
8. Mattle HP, Wentz KU, Edelman RR, et al. **Cerebral venography with MR.** *Radiology* 1991;178:453–458
9. Casey SO, Alberico RA, Patel M, et al. **CT cerebral venography.** *Radiology* 1996;198:163–170
10. GE Medical Systems. ***Advantage Windows 3D Analysis Package Tutorial/Cookbook.*** Rev. 1. Milwaukee, WI: GE Medical Systems; 1993:5–5
11. Anderson CM, Saloner D, Tsuruda JS, Shapeero LG, Lee RE. **Artifacts in maximum-intensity-projection display of MR angiograms.** *AJR Am J Roentgenol* 1990;154:623–629
12. Kamada K, Takeuchi F, Kuriki S, Oshiro O, Houkin K, Abe H. **Functional neurosurgical simulation with brain surface magnetic resonance images and magnetoencephalography.** *Neurosurgery* 1993;33:269–272
13. Fitzgerald DB, Cosgrove GR, Ronner S, et al. **Location of language in the cortex: a comparison between functional MR imaging and electrocortical stimulation.** *AJNR Am J Neuroradiol* 1997;18:1529–1539
14. Sisodiya SM, Stevens JM, Fish DR, Free SL, Shorvon SD. **The demonstration of gyral abnormalities in patients with cryptogenic partial epilepsy using three-dimensional MRI.** *Arch Neurol* 1996; 53:28–34
15. Katada K. **MR imaging of brain surface structures: surface anatomy scanning (SAS).** *Neuroradiology* 1990;32:439–448
16. Tsuruda J, Saloner D, Norman D. **Artifacts associated with MR neuroangiography.** *AJNR Am J Neuroradiol* 1992;13:1411–1422
17. Jacobs K, Moulin T, Bogousslavsky J, et al. **The stroke syndrome of cortical vein thrombosis.** *Neurology* 1996;47:376–382